Interband transitions in $In_xGa_{1-x}As/In_{0.52}Al_{0.48}As$ single quantum wells studied by room-temperature modulation spectroscopy

A. Dimoulas, J. Leng,* and K. P. Giapis†
Foundation for Research and Technology–Hellas, P.O. Box 1527, Heraklion 71110, Crete, Greece

A. Georgakilas
College of Engineering, University of Maryland, College Park, Maryland 20742

C. Michelakis
Foundation for Research and Technology–Hellas, P.O. Box 1527, Heraklion 71110, Crete, Greece

A. Christou
College of Engineering, University of Maryland, College Park, Maryland 20742
(Received 22 November 1991; revised manuscript received 9 November 1992)

Room-temperature phototransmittance and electrotransmittance of single quantum wells of $In_xGa_{1-x}As$ with $In_{0.52}Al_{0.48}As$ barriers have been used to study the excitonic interband transitions between the confined conduction- and valence-band states. Peak assignment has been confirmed by photocurrent spectroscopy. The lattice-matched ($x=0.53$) and strained ($x=0.6$) structures were considered for two different well widths of 50 and 250 Å. Transition energies and broadening parameters were measured from the spectra of the wide well samples and studied as a function of the principal quantum number. Reasonably good agreement between theory and experiment has been achieved by using published values of the electronic band-structure parameters. An observed monotonic increase of the linewidth with the quantum number has been associated with the presence of well-width fluctuations due to rough interfaces.

I. INTRODUCTION

Electric field modulation of reflectance and absorption has been extensively used during the last few years for the characterization of single (SQW) and multiple (MQW) quantum-well structures at room temperatures. Early works on electroreflectance have shown the effectiveness of this technique in studying the quantum confined carrier states in $GaAs/Al_xGa_{1-x}As$ SQW's and MQW's.[1–3] A contactless version of electric field modulation involves the alteration of the surface built-in electric field by using a laser light (photoreflectance, phototransmittance). Glembocki *et al.*[4] first reported that photoreflectance at 300 K exhibits sharp, well-resolved spectra, corresponding to interband transitions between quantized electron and hole states in $GaAs/Al_xGa_{1-x}As$ MQW's and modulation-doped heterojunctions. Since then, photoreflectance has been used for the study of $In_xGa_{1-x}As/GaAs$ SQW's (Ref. 5) and superlattices,[6] and $GaAs/Al_xGa_{1-x}As$ coupled MQW's.[7] Little work has been performed on electromodulation in the $In_xGa_{1-x}As/In_xAl_{1-x}As$ quantum-well system. This material system shows promise in electronic and optoelectronic device applications. The large conduction-band discontinuity ($\Delta E_c=0.5$ eV) and the small effective mass of electrons in the $In_xGa_{1-x}As$ well, make this heterostructure system attractive for the fabrication of high-performance electronic devices such as the high electron mobility transistors.[8] In addition, because of the small band gap of $In_xGa_{1-x}As$ alloys, optoelectronic devices[9] based on the above system can operate at long wavelengths (1.55 μm) suitable for optical fiber communication applications. The first observation by absorption spectroscopy of room-temperature excitonic interband transitions in $In_xGa_{1-x}As/In_xAl_{1-x}As$ MQW's was reported by Weiner *et al.*[10] Since then, the system has been studied by various optical techniques including photoluminescence,[11–13] photoluminescence excitation,[13] absorption,[14] and photocurrent spectroscopy.[15] Photoreflectance has been used to measure the band-gap energy of the bulk lattice-matched[16] and tensily strained[17] $In_xGa_{1-x}As$ on InP material. Using electroabsorption at 2 K, Satzke *et al.*[18] have examined lattice-matched $In_{0.53}Ga_{0.47}As/In_{0.52}Al_{0.48}As$ MQW's and superlattices. Electroreflectance at 300 K was used by Fritz *et al.*[19] to probe strained MQW's.

In the present work, we investigate the interband transitions in lattice-matched and strained $In_xGa_{1-x}As/In_xAl_{1-x}As$ SQW's by phototransmittance and electrotransmittance measurements at room temperature. Photocurrent spectroscopy on the same samples has been used to confirm peak assignment. The large number of the observed transition in thick QW's provided information in support of previously reported conduction- and valence-band offsets and effective masses of carriers in the $In_xGa_{1-x}As$ QW's. Linewidth analysis of the excitonic resonances improved insight into factors, such as interface roughness,[20,21] which affect the performance of optoelectronic devices.

II. EXPERIMENTAL DETAILS

The SQW's were grown by molecular-beam epitaxy on n^+-type InP(001) substrates and they had the following structure: (0.3 μm) $In_{0.52}Al_{0.48}As/(L_w)$ $In_xGa_{1-x}As/(1.0\ \mu m)$ $In_{0.52}Al_{0.48}As/n^+$-type InP(001). The $In_xAl_{1-x}As$ is the barrier while the $In_xGa_{1-x}As$ layer is the quantum-well region. Two samples with quantum-well thickness of $L_w = 50$ and 250 Å were produced for the lattice-matched nominal In composition of $x = 0.53$. Another sample with a width of 250 Å was prepared for the strained In composition of $x = 0.6$ (see Table I). The growth temperature of $In_xGa_{1-x}As$ and $In_xAl_{1-x}As$ layers was 500 °C. The samples were unintentionally doped n type to about 10^{15} cm^{-3}. The In composition $x = 0.6$ was chosen because compressive strain build-up in the $In_xGa_{1-x}As$ layer is beneficial to the performance of high electron mobility transistors grown on InP substrates.[8] The MQW structures are more suitable for optical device applications, due to their strong excitonic resonances at room temperature. However, by studying here the SQW structure, we avoid any complexities to the linewidth arising from interwell width variations. The quantum wells were characterized by photoluminescence (PL) and they were found to be of high quality. Indicatively, the PL full width at half maximum of the lattice-matched 50-Å quantum well was 9.5 meV at 12 K, which compares favorably to the best reported values.[11,14]

In the phototransmittance (PT) experimental arrangement, the transmittivity of the QW was modulated by a 10-mW He-Ne laser chopped at a frequency of 220 Hz. Light was detected by an EG&G $In_xGa_{1-x}As$ p-i-n photodiode operating in the photovoltaic mode. The ac part of the transmitted light, which is proportional to the transmittivity changes ΔT, was detected by a lock-in amplifier tuned at the modulating frequency. The dc part, proportional to the transmittivity T, was measured by a voltmeter. By using a double grating $\frac{1}{4}$ m SPEX monochromator to analyze incident light, the normalized quantity $\Delta T/T$ was finally obtained as a function of photon energy. A widely accepted modulation mechanism[22,23] involves electrons and holes, generated by the laser light, which move, under the influence of the built-in surface electric field, in such a way so that they neutralize it. Since, in many cases (including our case), the surface electric field penetrates into the QW region, the photogenerated carriers lead to an electric field modulation of the complex dielectric function or the absorption coefficient.[24,25] In the electrotransmittance configuration, the modulating source was a square wave voltage of frequency 300 Hz and peak-to-peak amplitude of 0.25 V, provided by a voltage generator. The ac bias was applied on a semitransparent Schottky contact made of Ti on the top $In_xAl_{1-x}As$ layer. The contact was 100 Å thin and 500 μm wide in diameter. The spectral range covered in the electromodulation experiments was from 0.7 to 1.35 eV. The lower limit was due to the limited response of the photodiode, while the upper limit was determined by the onset of absorption from the InP substrate. Photocurrent (PC) spectra were taken by focusing

TABLE I. Experimental and theoretical values of the interband transition energies for the three quantum wells studied. The experimental data are obtained from fitting of the phototransmittance spectra, while the corresponding theoretical values are calculated by using a finite square-well potential model, as described in the text.

Sample	X_{In}	L_w (Å)	E_A (eV)		$E_{A'}$ (eV)		E_B (eV)		E_C (eV)		E_D (eV)		E_E (eV)		E_F (eV)		E_G (eV)	
			Expt.	Theor.	Expt.	Theor.	Expt.	Theor.	Expt.	Theor.	Expt.	Theor.	Expt.	Theor.	Expt.	Theor.	Expt.	Theor.
S1	0.53	250	0.751	0.756 (11*h*)			0.789	0.792 (22*h*)	0.848	0.851 (33*h*)	0.924	0.933 (44*h*)	1.009	1.038 (55*h*)	1.1	1.155 (66*h*)	1.204	1.301 (77*h*)
S2	0.60	250	0.705	0.706 (11*h*)			0.755	0.745 (22*h*)	0.822	0.811 (33*h*)	0.906	0.902 (44*h*)	1.01	1.018 (55*h*)				
S3	0.53	50	0.907	0.895 (11*h*)	0.96	0.943 (11*l*)												

monochromatic light on the Schottky region and the photogenerated current was measured by the lock-in amplifier. The experimental error in the measurements of transition energies and broadening parameters was dominated by the resolution of the monochromator limited to 2 nm.

III. RESULTS AND DISCUSSION

A. Description of the phototransmittance spectra

The room-temperature PT spectra of the three SQW's are shown in Figs. 1–3. The PC spectra are placed on the same graphs for comparison. There exists a one-to-one correspondence between the peaks of PT and PC. Since electromodulation gives derivative line shapes,[23,24] the determination of the transition energies by a simple inspection of the spectra is not straightforward. A fitting procedure, as described in Sec. III B, is required. Transition energies are then determined as adjustable parameters from the fit. These are marked by small vertical lines, labeled by capital letters. They are also listed in Table I along with theoretically predicted values according to a model,[26] described in Sec. III C. These optical excitations are attributed to parity allowed transitions of the type *nnh* between states in the valence and conduction bands having the same quantum number *n*. (The transitions are labeled by using the notation *nmx*, where *n* and *m* are the principal quantum numbers of the electron and hole states, respectively, and $x=h$ or $x=l$ indicate the heavy- or light-hole band.)

In the PC spectra of the narrow quantum well *S*3 ($x=0.53$), an excitonic resonance can be clearly seen for the lowest-energy transition ($11h$), which is marked by *A* in Fig. 3. This resonance corresponds very well to the positive peak of the PT signal. In the case of the wide well samples, shown in Figs. 1 and 2, no excitonic peaks

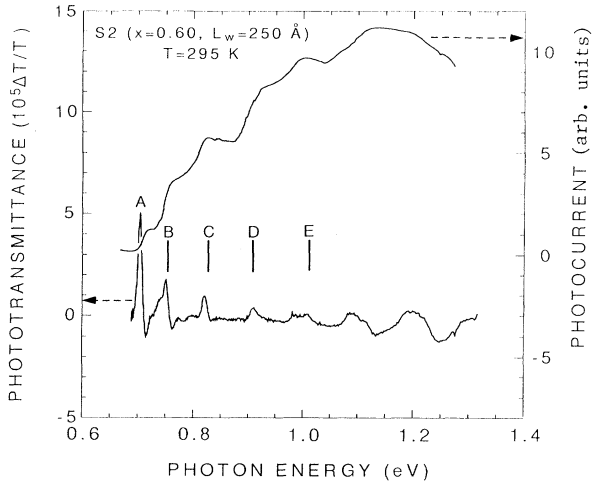

FIG. 2. Phototransmittance and photocurrent spectra, for the strained wide QW, at 295 K. Transition energies are marked by the labeled vertical lines.

can be seen in the PC spectra, presumably due to the weaker confinement of excitons in the wells. The steplike structure shows the onset of the absorption at each subband, while the plateaus are indicative of the constant two-dimensional joint density of states.[27] In the wide well samples ($L_w=250$ Å), a large number of interband excitonic transitions between quantum confined states were clearly resolved at the room-temperature PT spectra, as it is shown in Figs. 1 and 2. In sample *S*1 ($x=0.53$), as many as seven transitions are clearly observed. In sample *S*2 ($x=0.6$), five transitions are seen

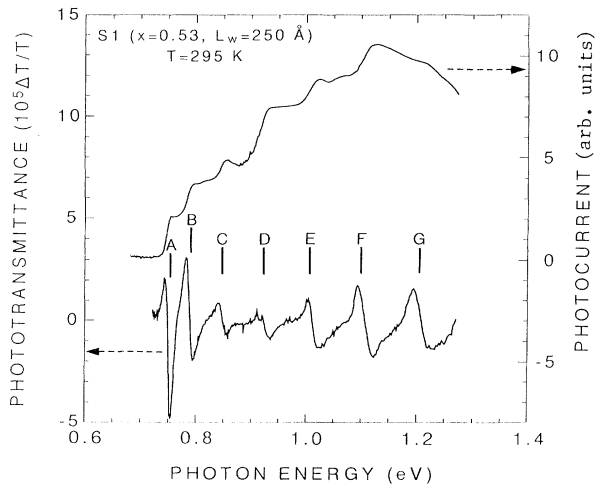

FIG. 1. Phototransmittance (PT) and photocurrent spectra, for the lattice-matched wide QW, at 295 K. The labeled vertical lines correspond to transition energies determined from the fitting of the PT data by using a Gaussian absorption profile.

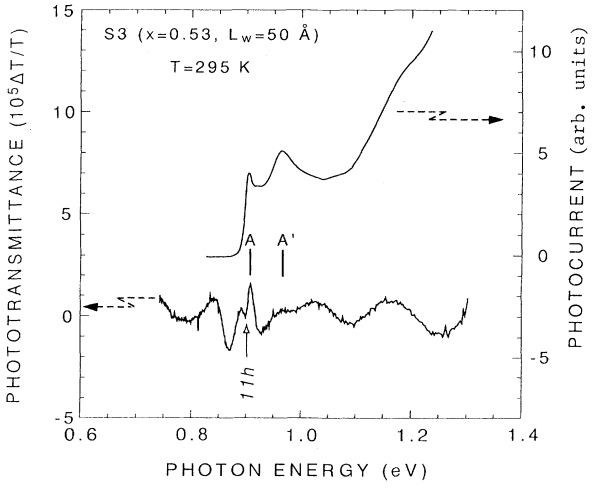

FIG. 3. Phototransmittance (PT) and photocurrent (PC) spectra of the lattice-matched narrow QW, at 295 K. *A* indicates the position of the lowest PT peak, while the arrow marks the position of the $11h$ transition, calculated from the theory. *A'* corresponds to the energy of the $11l$ transition, better resolved in the PC spectrum.

while another two at higher energies appear much broader and cannot be clearly resolved. In the same sample, weaker features appearing as low-energy shoulders to the main peaks may be attributed to normally parity forbidden transitions[28] of the type $nn'h$ between states of different quantum numbers. The effects of an externally applied dc bias on the behavior of the allowed and forbidden transitions have been discussed elsewhere.[30]

In sample $S3$ ($x=0.53$), only the $11h$ transition, marked by A in Fig. 3, can be seen at 0.907 eV. This is in agreement with theoretical predictions that only the lowest electron energy level forms a bound state in such narrow QW's. Following a finite square-well potential model[26] (see Sec. III C), the theoretically predicted energy for the $11h$ transition is 0.895 eV, marked by an arrow in Fig. 3. The agreement between theoretical and experimental values is satisfactory, considering that the energy position is very sensitive to the well width for such narrow quantum wells. A broad peak A', appearing in the PC spectrum at about 50 meV higher in energy than peak A, is assigned to the light-hole transition $11l$, in agreement with our model predictions. The same energy separation of 50 meV between $11h$ and $11l$ transitions, due to quantum confinement, has been recently predicted by Fritz *et al.*[19] It is remarkable, however, that this transition appears to be very weak in the PT spectrum of Fig. 3 so that it would be impossible to identify it without the help of the PC data. Indeed, no clear evidence of light-hole transitions in any of the four samples examined by PT and electrotransmittance (ET) was obtained, in agreement with previous observations[18] by electromodulation spectroscopy on the $In_xGa_{1-x}As/In_xAl_{1-x}As$ QW system. In sample $S3$, the baseline had an oscillatory structure (see Fig. 3). This is considered to be an interference effect of multiple reflections between the epilayer/substrate and epilayer/air interfaces prior to transmission of light through the InP substrate. Constructive interference occurs whenever the path difference $2d$ (d is the overall epilayer thickness) is equal to an integer multiple of the wavelength of incident light. This corresponds to an energy separation between the maxima of approximately $\Delta E = hc/2dn = 130$ meV, in very good agreement with the period of oscillations of 135 meV, measured from the spectrum of Fig. 3. Here, we have used the value $d = 1.3$ μm, estimated from the growth conditions and also we have assumed $n = 3.6$ for the refractive index. The oscillatory behavior of the background is more prominent in the photoreflectance spectra, which are not shown here. The sharp negative peak which appears close to the $11h$ (peak A), at the low-energy side, is probably due to the overlapping of peak A and the oscillatory background. It cannot be attributed to any particular interband transition and this can be further justified by the photocurrent spectra which show an onset of absorption at an energy corresponding to the spectral position of peak A.

It is worth noticing a difference between the phototransmittance and electrotransmittance spectra for sample $S1$ shown in Figs. 1 and 5, respectively. The last three transitions in the former have abnormally large intensities, in contrast with the latter, where the intensities

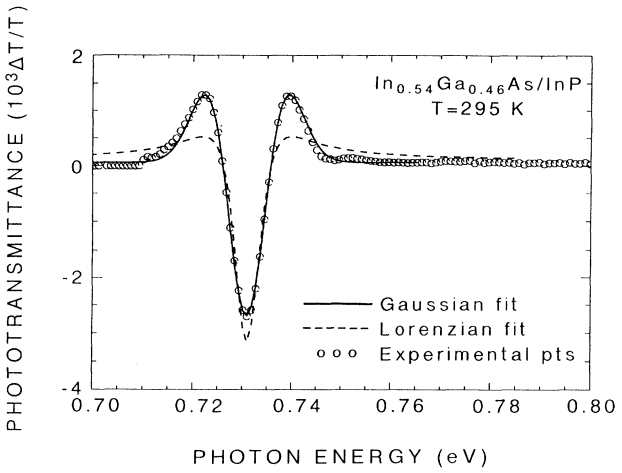

FIG. 4. Phototransmittance spectrum of bulk material at room temperature, fitted by Gaussian and Lorentzian absorption profiles for comparison.

decrease monotonically with the quantum number n. This could be attributed to the fact that light-induced modulation of the built-in electric field is not as effective in modulating the transmittivity as an externally applied voltage. Despite the difference in the behavior of peak intensity between PT and ET spectra, the line shapes and the energy positions of the corresponding spectral features are the same. This implies that the PT peaks are of the same origin as that of ET ones. The latter have clear derivative line shapes and exhibit the expected behavior of decreasing intensity for large n so that there is little doubt that ET, and hence PT signals, are due to interband transitions, while the possibility that they originate from interference oscillations can be excluded. This is further supported by the close correspondence between the electromodulation and the PC peaks apparent in Figs. 1–3, considering the fact that the steplike features in PC

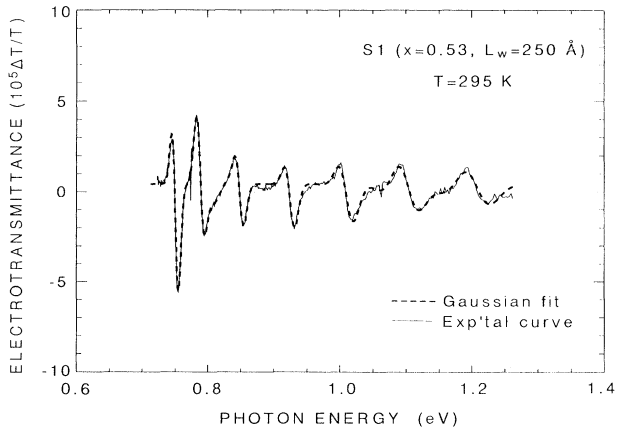

FIG. 5. Electrotransmittance from the lattice-matched sample $S1$, at 295 K, fitted by assuming a Gaussian absorption profile.

can never be due to optical interference.

Finally, it is worth mentioning that several measurements at different points across the wafers were performed in order to account for any inhomogeneities. No important differences between the spectra were observed and the transition energies did not change from point to point on the sample. In this way, the reproducibility of the data and the accuracy of the measurement of the parameters are ensured.

B. Line-shape analysis

The room-temperature PT spectra have a complex line shape, consisting of more than one peak. This complexity poses difficulties in obtaining the transition energies directly from the spectra. A fitting procedure is required, in which the energy, the lifetime, and the intensity of the transition are treated as adjustable parameters. When multilayer structures are probed by photoreflectance, interference oscillations due to multiple reflections on internal interfaces result in a spurious background. In addition, changes in the real and imaginary parts of the dielectric function both contribute to the PR line shape, making spectral analysis difficult.[31,32] Since the InP substrate is transparent in the wavelength region of interest, running the experiment in the transmittivity mode (phototransmittance) minimizes the above effects, which greatly simplifies the fitting process. Indeed, the relative change of transmittivity $\Delta T/T$ is determined by the change of the imaginary part of the dielectric function or, equivalently, by the change $\Delta\alpha$ of the absorption coefficient:[33]

$$\frac{\Delta T}{T} \simeq -L\Delta\alpha \ , \tag{1}$$

where L is the modulation depth, essentially equal to the depletion region.

In the present work, the photoinduced changes $\Delta\alpha$, associated with a single resonance, will be described in terms of first derivatives of the absorption coefficient α with respect to the energy E_0, the inverse lifetime Γ, and the intensity I of the excitonic transition:[24]

$$\Delta\alpha = \frac{\partial\alpha}{\partial E_0}\Delta E_0 + \frac{\partial\alpha}{\partial\Gamma}\Delta\Gamma + \frac{\partial\alpha}{\partial I}\Delta I \ . \tag{2}$$

Absorption[34] and photoreflectance measurements in $GaAs/Al_xGa_{1-x}As$ MQW's (Refs. 25, 31, and 35) and superlattices[7] have demonstrated that a Gaussian absorption function describes better the 300-K spectra, as compared to the more frequently used Lorentzian function. Gaussian-broadened excitonic absorption at 300 K is justified in view of thermal lattice disorder caused by LO phonons, as it was first discussed by Toyozawa.[36] Structural disorder on the atomic scale (interface roughness)[20,21] is taken into account by convoluting[37] the thermally broadened absorption with a Gaussian distribution of well-width fluctuations. The result is a Gaussian function[38]

$$\alpha = \frac{I}{\sqrt{2\pi}\Gamma} e^{-(\hbar\omega - E_0)^2/2\Gamma^2} \tag{3}$$

in which thermal effects and interface roughness contribute separately by Γ_T and Γ_r, respectively, to the total standard deviation Γ,

$$\Gamma = (\Gamma_T^2 + \Gamma_r^2)^{1/2} \ . \tag{4}$$

The latter is a measure of the linewidth broadening and, in the following, it will be referred to as the broadening parameter. Except from SQW's, we have also measured the bulk $In_{0.54}Ga_{0.46}As/InP$ system for comparison. In Fig. 4, room-temperature PT data from the bulk material are fitted by a Gaussian and a Lorentzian. The latter gives a very poor fit especially at the "wings" of the spectra. On the contrary, the Gaussian function gives an excellent fit with $E_0 = 0.731$ eV and broadening parameter $\Gamma = 4.9$ meV, which gives the contribution of thermal effects to the linewidth. It is expected that the Gaussian character of the absorption profile will be even more pronounced in SQW's, since interface roughness results in random fluctuations of the well width with a Gaussian distribution.

Interband transition energies and broadening parameters have been determined by fitting the electrotransmittance spectra of SQW's with the set of equations (1)–(4) and their values are given in Table I. It has to be mentioned here that since ET and PT are equivalent measurements it would be redundant to model both of them. Therefore, ET was chosen for the modeling since the latter exhibited clear, less noisy, and well-resolved spectra. The ET spectrum of sample $S1$ is typically shown in Fig. 5, represented by the solid line. The fitting curve is shown with the dashed line. The first term in Eq. (2), which gives the modulation of α with respect to the energy E_0 of the transition, is the dominant term in describing the ET spectra of all the SQW's.[24] This means that the dominant modulation mechanism involves the alteration of the energy of the confined states by the electric field via the quantum confined stark effect (QCSE).[39] A small contribution from the other terms in Eq. (2) is needed in order to describe the slight asymmetry with respect to the baseline which appears in some of these peaks. It is worth noticing the large difference between the bulk (Fig. 4) and SQW PT line shapes. In the latter case, the line shape consists of a positive and a negative peak, symmetrically placed with respect to the baseline, as compared to the large negative peak in the former case. For the bulk case, it suffices to consider only the derivative with respect to the broadening parameter Γ in order to describe adequately the whole spectrum. This is expected since exciton lifetime in the bulk is very sensitive to changes in the surface electric field. An increase of the electric field leads to exciton ionization with a consequent increase of the linewidth broadening. In SQW's, the presence of the barriers inhibits field-induced exciton ionization and the modulation of the transition energy due to the QCSE becomes the dominant mechanism.

This fitting procedure is proven useful in distinguishing between the various modulation mechanisms which give further information on the physical processes involved in the electromodulation of bulk and low dimensionality structures. A careful line-shape analysis is also needed in

order to extract information on the factors which influence the linewidth of the spectra. It is remarkable that our room-temperature phototransmittance and electrotransmittance spectra include a large number of well-resolved peaks, corresponding to higher-energy QW transitions. This gives us the opportunity to systematically study, in the next section, the dependence of the peak broadening on quantum number and correlate it to the presence of interface roughness[21] in the quantum wells.

C. Interband transitions and broadening parameters—a comparison with theory

A comparison of the experimentally measured transition energies with theory predictions is expected to provide valuable information on band-structure parameters, such as the band offset, effective mass, and energy gap of the $In_xGa_{1-x}As/In_{0.52}Al_{0.48}As$ heterostructure, at 300 K. We treat carriers within the effective-mass approximation and we use a simple finite square-well model, first described by Bastard and Brum,[26] in order to calculate the energy of the confined states of electrons and holes. Exciton binding energy has not been taken into account in the present calculation. Nevertheless, this does not modify significantly the results for the 250-Å wells since the exciton binding energy is less than 4 meV in such thick QW's.[40] Also, valence-band mixing effects have not been considered here. The results of the calculation and the experimental values are summarized in Table I, while the band-structure parameters used are listed in Table II.

An important parameter in the calculation is the barrier height for electrons and holes, which was set equal to the conduction- and valence-band discontinuity, respectively. Our experiments provide a set of data, which could be used in order to determine band discontinuities. However, it is not a purpose of this work to propose new values for these parameters. Our effort has rather been concentrated on fitting our experimental data by using already existing parameters, taken from the literature. This procedure could provide a further check of the validity of the band offset values that have been previously reported.

Based on capacitance-voltage measurements, People *et al.*[41] gave a value of 0.5 eV for the conduction-band discontinuity of the lattice-matched heterostructure. Other workers have found this value to agree well with their experimental data.[9,15,18] Therefore, we use it in the present work in order to calculate the transition energies for the case $x=0.53$. As indium composition in the well increases, the conduction-band discontinuity also increases, presumably due to the smaller band gap of $In_xGa_{1-x}As$. For the case $x=0.6$, a value $\Delta E_c=0.55$ eV is used, in accordance with recent reports for the same heterostructure system.[19]

The results of the calculation and the experimental data are plotted on the same graph in Fig. 6, where the variation of the transition energies with the quantum number n is shown for the two wide well samples. The lattice-matched sample $S1$ corresponds to the energy scale on the left axis while the strained sample $S2$ is to be read on the right axis. Symbols represent experimental data taken from Table I, while the small horizontal lines correspond to the theoretical points, obtained by using the aforementioned finite square-well potential model.[26] On the same graph, the solid lines indicate the quadratic dependence $E_n=E_g+\hbar^2\pi^2n^2/2\mu L_w^2$, in an infinite square-well potential approximation, where E_g is the band-gap energy of $In_xGa_{1-x}As$ and $\mu=m_e^*m_h^*/(m_e^*+m_h^*)$ is the interband reduced effective mass. When using infinite barriers, the square-well model gives a good prediction of the ground $11h$ transition but it departs rapidly from the experimental points at higher energies. By using finite barrier heights though, a better agreement with the experiment is obtained, as demonstrated by the horizontal lines in Fig. 6. For sample $S1$, the model predicts correctly the first four transitions but overestimates the energies of the remaining three transitions at larger quantum numbers. The failure of the model at higher energies may be explained by the fact that the effective-mass approximation is insufficient to describe electron and hole states at this energy range. It is possible that consideration of band nonparabolicity effects may lead to an improved model. The same problem was faced by Satzke *et al.*[18] in their low-temperature electroabsorption data of 138- and 103-Å-thick MQW's. These workers, in an attempt to remove the discrepancy between theory and experiment, have considered nonparabolic bands within Kane's approximation,[42] but with little success. They found it necessary to consider a linearly increasing electron effective mass with energy in order to match their experimental results. In our case, it is interesting to notice that a better agreement between theory and experiment is obtained for the sample $S2$ with In composition $x=0.6$. An explanation may be based on the fact that the QW depth increases as a result of the band gap lowering at higher In concentrations. Our analysis predicts that the higher-energy states are more sensitive to the choice of band offsets and effective masses compared to the lowest two or three states. This demonstrates the importance of observing the higher-lying tran-

TABLE II. Band-structure parameters used in the finite square-well potential model calculations.

	E_g (eV)		ΔE_c (eV)			
	$x=0.53$	$x=0.6$	$x=0.53$	$x=0.6$	m_e^*/m_e	m_{hh}^*/m_e
$In_xGa_{1-x}As$	0.745[a]	0.692[a]	0.50[b]	0.55[c]	0.041[d]	0.377[e]
$In_{0.52}Al_{0.48}As$		1.46[f]			0.075[e]	0.57[e]

[a]Reference 46.
[b]Reference 41.
[c]Reference 19.
[d]Reference 50.
[e]Reference 15.
[f]Reference 51.

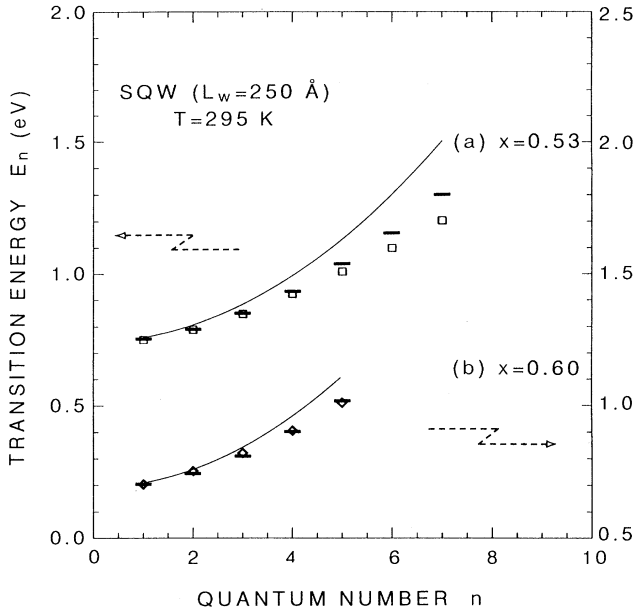

FIG. 6. Transition energies versus the quantum number for (a) the lattice-matched and (b) the strained wide QW's, at 295 K. Symbols denote experimental points. Horizontal bars indicate theoretical positions according to a finite square-well potential model and solid lines describe predictions of an infinite square-well potential.

sitions in the modulation spectra, in order to check the validity of the band-structure parameters used in such calculations.

The band-gap energy E_g of $In_xGa_{1-x}As$ is another quantity which needs careful consideration. Different room-temperature E_g values, in the range between 0.73 and 0.75 eV, have been obtained from photoluminescence,[37,43] photoreflectance,[16] and absorption[44] measurements for the lattice-matched $In_{0.53}Ga_{0.47}As/InP$ bulk system. Calculation of E_g for a certain In composition x is based on a linear interpolation between the band-gap energies of the two constituent binaries. However, a non-negligible quadratic term, whose coefficient (the bowing parameter) is not well known, is also involved in the calculation. Early optical studies have produced values of the bowing parameters in the range between 0.36 and 0.5.[37,45] In the present work, we calculate $E_g(x)$ based on a formula of Ji *et al.*,[46] which uses the bowing parameter $C=0.45$, very close to the value of 0.475 derived by Goetz *et al.*[37] from their photoluminescence experiments. This formula gives a value $E_g=0.745$ eV for the lattice-matched composition $x=0.53$, which is very close to 0.75 eV reported by Goetz *et al.*[37] We consider the value $E_g=0.745$ eV to be a good estimate of the band-gap energy of the lattice-matched $In_xGa_{1-x}As$ material.

For In composition different from the lattice-matched $x=0.53$, the band-gap energy has to be corrected for strain that might be present in the material. In the case of sample $S2$ with $x=0.6$, the lattice mismatch, calculated from Vegard's law, is $\Delta a/a \simeq 4.5\times10^{-3}$. The absence of misfit dislocations in $S2$, verified by transmission electron microscopy, indicated that the mismatch is fully accommodated by coherent compressive strain ϵ, which is equal in magnitude to the lattice mismatch: $\epsilon=-\Delta a/a=-4.5\times10^{-3}$. The strain-induced band-gap energy shift ΔE_g,[47] associated with the heavy-hole state, can be calculated from

$$\Delta E_g=2\alpha(1-C_{12}/C_{11})\epsilon-b(1+2C_{12}/C_{11})\epsilon\ .$$

The stiffness coefficients are taken to be $C_{11}=10.29\times10^{11}$ and $C_{12}=5.1\times10^{11}$ dyn/cm^2, while the hydrostatic and shear deformation potentials are given the values $\alpha=-7.45$ eV and $b=-1.75$ eV, respectively. All of them represent mean values between the corresponding binaries.[48] Strain shifts the band gap upwards to a value of 0.692 eV which is 18 meV larger than the unstrained value, obtained from the formula of Ji *et al.*[46] for $x=0.6$. By using $E_g=0.692$ eV, an excellent fit of the experiment was obtained for sample $S2$, as can be seen in Fig. 6.

The study of the influence of interface roughness to the linewidth of optical spectra has been limited so far to low-temperature photoluminescence measurements in which only the ground-state transition was involved.[21] The appearance of a large number of higher interband transitions, with well-resolved line shapes, in our room-temperature electrotransmittance spectra, permitted us to systematically study the dependence of the broadening parameter Γ on the quantum number n. We have chosen to examine only the lattice-matched QW $S1$, in order to avoid any contributions from strain in the sample with $x=0.6$. The broadening parameters, measured from the fitting of the spectra with the Gaussian of Eq. (3), are denoted by symbols in Fig. 7. It can be seen from this figure that for small quantum numbers up to $n=3$, Γ remains approximately constant. For larger quantum numbers, Γ increases rapidly, spanning the range from 5 meV for $n=1$ up to 14 meV for the highest transition $n=7$.

There exists clearly a superlinear relationship between Γ and n, which could be fitted by many models with proper adjustable parameters. However, Eq. (4) is suggestive of thermal and interface roughness contributions to the linewidth. The latter effect can be understood by considering that small fluctuations ΔL_w of the well width obeying a Gaussian distribution, result in corresponding fluctuations ΔE_n of the transition energies,[20,21] which can be obtained to the first order from $\Delta E_n=(dE_n/dL_w)\Delta L_w$. In the infinite square-well potential approximation, there is a quadratic dependence of the transition energies on n, so that, according to the former relation, the standard deviation Γ_r associated with interface roughness can be expressed in a simple form as[21]

$$\Gamma_r=\delta_l\frac{\hbar^2\pi^2}{\mu L_w^3}n^2\ , \tag{5}$$

where δ_l is the standard deviation of the well-width fluctuations.

By taking into consideration Eq. (4), the dependence of the total broadening parameter Γ to the quantum number

n can be expressed, in the infinite square-well approximation, as

$$\Gamma=\left[\Gamma_T^2+\delta_l^2\left[\frac{\hbar^2\pi^2}{\mu L_w^3}\right]^2 n^4\right]^{1/2}. \quad (6)$$

This equation is chosen for the description of the experimental results without the use of fitting parameters. In the absence of interface disorder ($\delta_l=0$) or in the limit of infinite well widths ($L_w\rightarrow\infty$), cases resembling that of the bulk material, Eq. (6) reduces to $\Gamma=\Gamma_T$. Therefore, it occurs naturally that Γ_T should be taken equal to 4.9 meV, which is the value of the thermal broadening parameter measured in the bulk $In_{0.54}Ga_{0.46}As/InP$ (see Fig. 4 and discussion in Sec. III B). The average well width L_w is set equal to 250 Å, while from Table II, the interband reduced effective mass is taken to be $\mu=0.037m_e$. The quantity δ_l can take any value larger than or equal to 2.6 Å, the separation between adjacent monolayers in the [100] direction. The variation of Γ with n, as described by Eq. (6), is plotted in Fig. 7 for two different values of $\delta_l=2.6$ Å (broken line) and $\delta_l=5.2$ Å (dash-dotted line) corresponding to average well-width fluctuations of one and two monolayers, respectively. It is remarkable that the theoretical line corresponding to $\delta_l=1$ monolayer follows closely the experimental points, although it predicts slightly higher values of the broadening parameter. The model clearly overestimates the influence of interface disorder, which is explained by the fact that Eq. (6) is only an approximation, valid when the square-well potential has infinite barriers. For finite barriers, which is the case here, the interface-roughness term is expected to vary more slowly than the n^2 dependence in Eq. (5), implying that the $\delta_l=1$ monolayer line will decline from, while the $\delta_l=2$ monolayers line will come closer to the experimental points. A more accurate analysis is hampered by the lack of an analytical expression in the case of finite square-well potential systems. However, we believe that the present approximate model captures the physical essence of the observed monotonic increase of the linewidth with n, identifying it as an interface-roughness effect. Furthermore, it facilitates an estimation of the average statistical well-width fluctuations to a value between one and two monolayers.

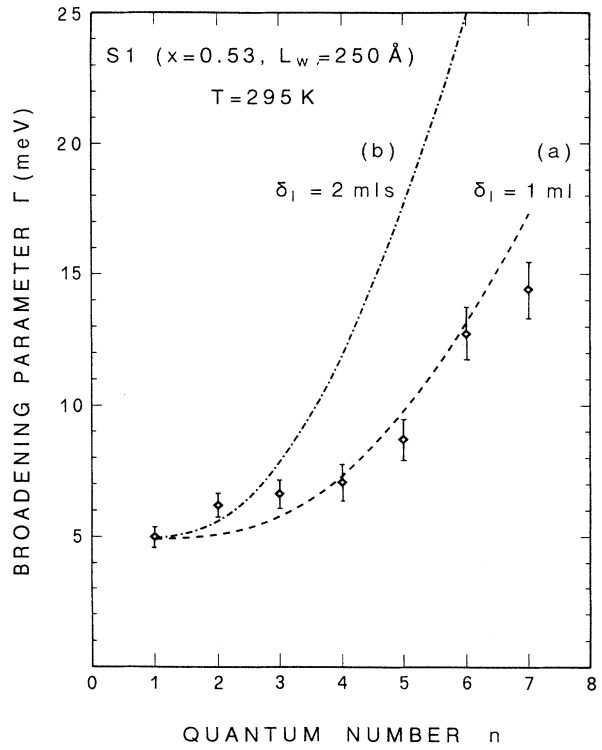

FIG. 7. The broadening parameter vs the quantum number for the lattice-matched wide QW, at 295 K. Symbols denote experimentally obtained values. The lines represent a theoretical model that takes into account thermal effects and interface roughness. Two cases were considered differing by the value of the average well-width fluctuation δ_l: (a) The broken line corresponds to $\delta_l=2.6$ Å (one monolayer). (b) The dash-dotted line corresponds to $\delta_l=5.2$ Å (two monolayers).

In the aforementioned analysis, it was assumed that the thermal broadening effects, fully accommodated in the term Γ_T^2 of Eq. (6), have the same influence to the linewidth of the resonance for all n. Although this may not be strictly true, it is argued that thermal effects cannot account for the observed strong dependence of Γ on the quantum number. Indeed, if this were the case, then the last transition ($n=7$), which approaches the bulk situation closer than any other transition, should exhibit a broadening close to that of the bulk material. However, the latter having typically $\Gamma\simeq 5$ meV is much more narrow than the former with $\Gamma\simeq 14$ meV, and instead it has a linewidth almost the same as that of the first ($n=1$) transition (Fig. 7). This implies that a mechanism other than the exciton-phonon interaction is responsible for the excess broadening at higher values of n. The frequently observed inferior quality of the barrier material [alloy disorder and clustering in $In_xAl_{1-x}As$ (Ref. 49)] may be considered as a source of linewidth broadening. However, this effect is relatively unimportant in thick QW's ($L_w>200$ Å), since the penetration of the exciton wave function in the barrier is negligible.[49] Finally, we note that the first three transitions in Fig. 7 have a broadening parameter approximately equal to the bulk value. This is in agreement with theoretical predictions[49] that the ground-state exciton for thick (>200 Å) QW's is insensitive to interface imperfections, contrary to what happens in thinner QW's where the contribution of interface-roughness is significantly larger. This is predicted from Eqs. (5) and (6), and confirmed by experimentally measuring an increased value of 8.5 meV for the broadening parameter of the $11h$ transition in the 50-Å QW ($S3$).

A similar dependence of the broadening parameter on the quantum number has been found by Miller *et al.*[28] in studying 100-Å-thick $GaAs/Al_xGa_{1-x}As$ MQW's. Their work, however, was based on photoluminescence and photoluminescence excitation spectroscopy at low temperature. They found that Γ showed an increasing behavior with the quantum number following a simple formula: $\Gamma=Cn_en_h$, where C is a constant slightly less than unity. The quantum numbers n_e and n_h for electron

and hole states, respectively, are different from each other for the case of forbidden transitions. However, for allowed transitions $n_e = n_h = n$, so that Γ follows the same quadratic behavior as in Eq. (5). Although these workers were the first to deduce the quadratic dependence of Γ on n, they have not associated it to interface-roughness effects. In the present model, we have correlated the dependence of the broadening parameter on n to interface roughness and also included thermal effects, which are absent from low-temperature optical data. It is expected that our analysis will help in the interpretation of the spectral line shapes in electromodulation experiments, especially in cases where more than one broadening mechanism is involved. Furthermore, it provides a sensitive method for probing the quality of QW interfaces and complements results on the subject, previously assessed by luminescence methods alone.

IV. CONCLUSIONS

It has been shown that room-temperature phototransmittance and electrotransmittance are powerful techniques for the study of interband transitions in single quantum wells of $In_xGa_{1-x}As/In_xAl_{1-x}As$. They produce spectra, which are easy to interpret and analyze, since they are related only to changes in the imaginary part of the dielectric constant. Investigation of lattice-matched ($x=0.53$) and strained ($x=0.6$) $In_xGa_{1-x}As/In_{0.52}Al_{0.48}As$ single quantum wells by using these techniques, resulted in a systematic study of interband transitions for thin (50 Å) and thick (250 Å) confined layers. The numerous transitions, resolved in the spectra of the wide well samples, enabled modeling the dependence of allowed transition energies and broadening parameters on the quantum number. These parameters were determined by fitting the electrotransmittance spectra with a Gaussian absorption profile, Interband transition energies have also been calculated by using a finite square-well potential approximation and by taking into account compressive strain in calculating the energy gap of $In_xGa_{1-x}As$ for the case $x=0.6$. It was concluded that theory matches reasonably well the experiment, when the conduction-band discontinuity ΔE_c is set equal to 0.5 eV for the lattice-matched quantum well. A better matching between theory and experiment was obtained for the strained quantum well with the use of $\Delta E_c = 0.55$ eV. These values correspond to conduction-band offsets of 70% of the band-gap difference between $In_xGa_{1-x}As$ and $In_xAl_{1-x}As$ materials. The modulation experiments provided an additional means to test previously reported values for the conduction- and valence-band discontinuities, as well as other band-structure parameters. In the lattice-matched quantum well, the broadening parameter of the lowest two transitions was found to be close to the value obtained for bulk $In_xGa_{1-x}As$, implying that these transitions are insensitive to any imperfections at the heterointerfaces. This agrees well with previous theoretical predictions for thick quantum wells that interface roughness does not have a significant contribution to the linewidth of the ground-state excitonic transition. The higher-lying transitions, however, showed an increased broadening with a superlinear dependence on the quantum number n, which was considered to be an effect of the presence of random well-width fluctuations. Our treatment was general enough to allow distinction between thermal and interface-roughness broadening mechanisms, each one contributing separately to the linewidth of the room-temperature modulation spectra.

ACKNOWLEDGMENTS

The present work was supported by the European Economic Communities Basic Research Program No. ESPRIT 3086. One of us (A.D.) wishes to thank Professor Fred H. Pollak, Professor G. Guillot, Dr. O. J. Glembocki, and Dr. P. Lefebvre for useful discussions.

*Permanent address: Zhenjiang Shipbuilding Institute, People's Republic of China.

†Present address: Division of Chemistry and Chemical Engineering, California Institute of Technology, Pasadena, CA 91125.

[1]E. E. Mendez, L. L. Chang, G. Landgren, R. Ludeke, L. Esaki, and F. H. Pollak, Phys. Rev. Lett. **46**, 1230 (1981).

[2]M. Erman, J. B. Theeten, P. Frijlink, S. Gaillard, H. J. Hia, and C. Alibert, J. Appl. Phys. **56**, 3241 (1984).

[3]P. C. Klipstein, P. R. Tapster, N. Apsley, D. A. Anderson, M. S. Skolnik, T. M. Kerr, and K. Woodbridge, J. Phys. C **19**, 857 (1986).

[4]O. J. Glembocki, B. V. Shanabrook, N. Bottka, W. T. Beard, and J. Comas, Appl. Phys. Lett. **46**, 970 (1985).

[5]A. Ksendzov, H. Shen, F. H. Pollak, and D. P. Bour, Solid State Commun. **73**, 11 (1990).

[6]C. Vazquez-Lopez, E. Ribeiro, F. Cerdeira, P. Motisuke, M. A. Sacilotti, and A. P. Roth, J. Appl. Phys. **69**, 7836 (1991).

[7]H. Shen, S. H. Pan, F. H. Pollak, M. Dutta, and T. R. AuCoin, Phys. Rev. B **36**, 9384 (1987).

[8]J. M. Kuo, M. D. Feuer, and T. Y. Chang, J. Vac. Sci. Technol. B **6**, 657 (1988).

[9]K. Wakita, Y. Kawamura, Y. Yoshikuni, H. Asahi, and S. Uehara, IEEE J. Quantum Electron. **QE-22**, 1831 (1986).

[10]J. S. Weiner, D. S. Chemla, D. A. B. Miller, T. H. Wood, D. Sivco, and A. Y. Cho, Appl. Phys. Lett. **46**, 619 (1985).

[11]D. F. Welch, G. W. Wicks, and L. F. Eastman, Appl. Phys. Lett. **46**, 991 (1985).

[12]R. Cingolani, W. Stolz, and K. Ploog, Phys. Rev. B **40**, 2950 (1989).

[13]W. Stolz, J. Wagner, and K. Ploog, J. Cryst. Growth **81**, 79 (1987).

[14]S. Gupta, P. K. Bhattacharya, J. Pamulapati, and G. Mourou, J. Appl. Phys. **69**, 3219 (1991).

[15]S. Nojima, Y. Kawamura, K. Wakita, and O. Mikami, J. Appl. Phys. **64**, 2795 (1988).

[16]D. K. Gaskill, N. Bottka, L. Aina, and M. Mattingly, Appl. Phys. Lett. **56**, 1269 (1990).

[17]E. H. Reihlen, D. Birkedal, T. Y. Wang, and G. B. Stringfellow, J. Appl. Phys. **68**, 1750 (1990).
[18]K. Satzke, G. Weiser, W. Stolz, and K. Ploog, Phys. Rev. B **43**, 2263 (1991).
[19]I. J. Fritz, J. F. Klem, T. M. Brennan, J. R. Wendt, and T. E. Zipperian, Superlatt. Microstruct. **10**, 99 (1991).
[20]J. Singh, K. K. Bajaj, and S. Chaudhuri, Appl. Phys. Lett. **44**, 805 (1984).
[21]M. A. Herman, D. Bimberg, and J. Christen, J. Appl. Phys. **70**, R1 (1991).
[22]J. L. Shay, Phys. Rev. B **2**, 803 (1970).
[23]F. H. Pollak and O. J. Glembocki, Proc. SPIE **946**, 2 (1988).
[24]B. V. Shanabrook, O. J. Glembocki, and W. T. Beard, Phys. Rev. B **35**, 2540 (1987).
[25]W. M. Theis, G. D. Sanders, C. E. Leak, K. K. Bajaj, and H. Morkoc, Phys. Rev. B **37**, 3042 (1988).
[26]G. Bastard and J. A. Brum, IEEE J. Quantum Electron. **QE-22**, 1625 (1986).
[27]G. Bastard, *Wave Mechanics Applied to Semiconductor Heterostructures* (Monographies de Physique, CEDEX, France, 1983), p. 13.
[28]R. C. Miller, A. C. Gossard, G. D. Sanders, Y-C. Chang, and J. N. Schulman, Phys. Rev. B **32**, 8452 (1985).
[29]Y-C. Chang and J. N. Schulman, Appl. Phys. Lett. **43**, 536 (1983).
[30]A. Dimoulas, K. P. Giapis, J. Leng, G. Halkias, K. Zekentes, and A. Christou, J. Appl. Phys. **72**, 1912 (1992).
[31]A. J. Shields, P. C. Klipstein, and N. Apsley, Semicond. Sci. Technol. **4**, 476 (1989).
[32]A. J. Shields and P. C. Klipstein, Phys. Rev. B **43**, 9118 (1991).
[33]M. Cardona, *Modulation Spectroscopy* (Academic, New York, 1969), Suppl. 11, p. 218.
[34]D. S. Chemla, D. A. B. Miller, P. S. Smith, A. C. Gossard, and W. Wiegmann, IEEE J. Quantum Electron. **QE-20**, 265 (1984).
[35]O. J. Glembocki and B. V. Shanabrook, Superlatt. Microstruct. **3**, 235 (1987).
[36]Y. Toyozawa, Prog. Theor. Phys. **20**, 53 (1958).
[37]K.-H. Goetz, D. Bimberg, H. Jurgensen, J. Selders, A. V. Solomonov, G. F. Glinskii, and M. Razeghi, J. Appl. Phys. **54**, 4543 (1983).
[38]A. Dimoulas, Ph.D. thesis, Physics Department, University of Crete, Greece, 1991 (in English).
[39]D. A. B. Miller, D. S. Chemla, T. C. Damen, A. C. Gossard, W. Wiegmann, T. H. Wood, and C. A. Burrus, Phys. Rev. Lett. **53**, 2173 (1984).
[40]S. Hong and J. Singh, J. Appl. Phys. **62**, 1994 (1987).
[41]R. People, K. W. Wecht, K. Alavi, and A. Y. Cho, Appl. Phys. Lett. **43**, 118 (1983).
[42]E. O. Kane, in *Semiconductors and Semimetals,* edited by P. K. Williardson and A. C. Beer (Academic, New York, 1966), Vol. 1.
[43]A. F. S. Penna, J. Shah, T. Y. Chang, and M. S. Burroughs, Solid State Commun. **51**, 425 (1984).
[44]E. Zielinski, H. Schweizer, K. Streubel, H. Eisele, and G. Weimann, J. Appl. Phys. **59**, 2196 (1986).
[45]A. G. Thompson and J. C. Woolley, Can. J. Phys. **45**, 255 (1967).
[46]G. Ji, D. Huang, U. K. Reddy, T. S. Henderson, R. Houdre, and H. Morkoc, J. Appl. Phys. **62**, 3366 (1987).
[47]F. H. Pollak, Surf. Sci. **37**, 863 (1973).
[48]S. Adachi, J. Appl. Phys. **53**, 8775 (1982).
[49]J. Singh and K. K. Bajaj, J. Appl. Phys. **57**, 5433 (1985).
[50]R. J. Nicholas, J. C. Portal, C. Houlbert, P. Perrier, and T. P. Pearsall, Appl. Phys. Lett. **34**, 492 (1979).
[51]D. Olego, T. Y. Chang, E. Silberg, E. A. Caridi, and A. Pinczuk, Appl. Phys. Lett. **41**, 476 (1982).